Journal of Power Sources 196 (2011) 10748–10752

Contents lists available at ScienceDirect

Journal of Power Sources

journal homepage: www.elsevier.com/locate/jpowsour

Short communication

Selenium: Another metalloid beneficial for the electrochemical performance of Co electrode in alkaline rechargeable batteries

Hongmei Du, Lifang Jiao*, Qinghong Wang, Qingna Huan, Wenxiu Peng, Dawei Song, Yijing Wang, Huatang Yuan

Institute of New Energy Material Chemistry, Key Laboratory of Advanced Energy Materials Chemistry (MOE), MOE (IRT-0927), Nankai University, Tianjin 300071, PR China

ARTICLE INFO

Article history:
Received 31 May 2011
Received in revised form 20 July 2011
Accepted 20 July 2011
Available online 27 July 2011

Keywords:
Se-incorporation
Alkaline rechargeable batteries
Cobalt-based materials
Electrochemical performance
Negative electrode material

ABSTRACT

Many inactive materials have been found to be helpful for improving the electrochemical performance of Co electrode in alkaline rechargeable batteries, including B, P, Si, S, Si_3N_4, and BN. In this paper we find for the first time that selenium has a similar effect with them. Selenium incorporation is realized through a liquid-reduction method. The obtained Co–Se sample is investigated as the negative electrode material of alkaline rechargeable battery. Experimental results demonstrate that the Co–Se sample electrode shows excellent electrochemical reversibility and considerably high charge–discharge capacity, showing a great potential to enhance the electrochemical performance of Co-based alkaline rechargeable batteries. The electrochemical reaction mechanism and function mechanism of Se are also investigated.

1. Introduction

With the development of science and technology, the need for electrical vehicles with high energy density has increased rapidly. Alkaline rechargeable nickel-based batteries including nickel/cadmium (Ni/Cd), nickel/iron (Ni/Fe), nickel/zinc (Ni/Zn) and nickel/metal hydride (Ni/MH) batteries have been widely investigated in the field of electric energy storing devices [1–11]. Among these batteries, Ni/Cd and Ni/MH batteries have been the most promising. For the high energy and power density with low cost, Ni/Cd batteries were widely used for a long time. However, due to the poisonous nature of cadmium to the environment, Ni/Cd batteries have been replaced. Ni/MH batteries using hydrogen storage alloys as the negative electrode materials have been drawing increasing attention due to their higher energy density both in terms of weight and volume, but the practical discharge capacity of commercial Ni/MH batteries is only about 330 mAh g^{-1} and has little room to be improved.

Recently, a new type of Co-based materials is reported to have high reversible discharge capacity and good cycle life as negative electrode materials of alkaline rechargeable batteries. The electrochemical performances of Cobalt-based materials electrodes are obviously improved after mixing some inactive materials (such as B, Si, P, BN, Si_3N_4, S, and CNTs) [12–22]. But the function mechanisms of the inactive materials on Co electrode is different. Some of them such as BN, Si_3N_4 and CNTs introduce a better distribution matrix for metallic Co [18,19,21]. Some elements such as B and S can dissolve in alkaline aqueous, resulting in the creation of newly built interspaces among the Co particles. The newly built interspaces increase the contact area between active electrode materials of the electrodes and alkaline electrolyte. So the efficiency of electrochemical reactions is thus enhanced, resulting in better electrochemical performance [21,24–26].

As we know, like B and S, selenium can also be dissolved in the alkaline solution. Besides, as a member of the semiconductor family, selenium has a better electrical conductivity than those previously reported S and B [27]. Based on these properties, we believe that Se is beneficial to improve the electrochemical performance of Co electrode in alkaline rechargeable batteries.

In this work, Co–Se sample was obtained by a liquid reduction method and used for the first time as a negative electrode material of alkaline rechargeable battery. Influence and function mechanism of Se on the electrochemical properties of Co was investigated systematically. The overall reaction mechanism of the Co–Se electrode was also discussed.

2. Experiment

2.1. Preparation and structural characterization

Co–Se sample was prepared by rapidly mixing two solutions for redox reaction under desired conditions. In a typical preparation

* Corresponding author. Tel.: +86 22 23498089; fax: +86 22 23502604.
E-mail address: jiaolf@nankai.edu.cn (L. Jiao).

0378-7753/$ – see front matter © 2011 Elsevier B.V. All rights reserved.
doi:10.1016/j.jpowsour.2011.07.068

procedure, firstly 1.000 g cobalt chloride and 0.727 g sodium selenite were dissolved in 20 ml anhydrous ethanol as part A. 1.000 g sodium hydroxide was dispersed in 20 ml hydrazine hydrate as part B. Then, part A and part B were mixed under vigorous stirring at 50 °C for 2 h. The precipitates were collected by centrifugation, and washed alternately with deionized water and ethanol for three times. After being dried in vacuum at 60 °C for 12 h, Co–Se sample was obtained. For comparison, Se–free Co sample was prepared by the same method without adding sodium selenite.

2.2. Compositional and structural characterization

The crystal structure and surface configuration of the samples were characterized by powder X-ray diffractometer (XRD, Rigaku D/max-2500 with Cu Kα radiation), scanning electron microscopy (SEM, JEOL JSM-6700F Field Emission) and energy dispersive X-ray spectrum (EDS, Kevex Sigma TM Quasar). The elemental composition of the Co–Se sample after cyclic voltammetry cycles was measured by inductive coupled plasma atomic emission spectroscopy (ICP-AES, USA Themo Jarrel-Ash). The chemical states of the sample after the first discharged state were investigated with XPS (PHI15300X).

2.3. Electrochemical measurements

Negative electrodes were constructed through mixing as-prepared materials with carbonyl nickel powders in a weight ratio of 1/3. The powder mixture was pressed under 30 MPa pressure into a small pellet of 10-mm diameter and 1.5-mm thickness. The pellet was incorporated into a nickel foam substrate of 2 cm × 2 cm in size. Electrochemical measurements were conducted in a three-compartment cell using Co and Co–Se samples as working electrodes, NiOOH/Ni(OH)$_2$ and Hg/HgO electrodes were used as the counter electrode and the reference electrode, respectively. The electrolyte solution was a 6 M KOH aqueous solution.

The cycle life and charge–discharge curves were tested in a three-compartment cell using a Land battery test instrument (CT2001A). The electrodes were charged at 100 mA g^{-1} for 5 h, then discharged at 50 mA g^{-1} to −0.5 V (vs. Hg/HgO). The interval between charge and discharge was 5 min. Zahner IM6e electrochemical workstation was used for cyclic voltammetry (CV, scan rate: 0.2 mV s^{-1}; potential interval: −1.2 to −0.4 V vs. Hg/HgO). All the tests were performed at room temperature.

To study the electrochemical reaction mechanism, the microstructures of the Co–Se sample electrode after different charged/discharged states were measured by XRD. In order to avoid the influence of the Ni diffraction peaks, the electrodes for XRD measurements were prepared by mixing Co–Se sample, acetylene black and polytetrafluoroethylene at the weigh ratio of 10:2:1 into a paste, which was roll pressed to 0.15-mm thick film and then pressed onto a porous nickel mesh. After electrochemical cycles, the samples at different discharged/charged states were taken from the cells, washed with distilled water and ethanol, and then dried in vacuum at 80 °C for 3 h.

3. Results and discussion

3.1. Material characterization

Fig. 1 shows the XRD patterns of the as-prepared Co and Co–Se samples. As it can be seen, most diffraction peaks of the Co sample can be indexed to hexagonal Co (JCPDS no. 89-4308) besides a small fraction of cubic Co (JCPDS no. 15-806). For the Co–Se sample, the position of the diffraction peaks is consistent with the Co sample, whereas the intensity is weakened, which is similar to the result of S incorporation [21]. In addition, there is a small peak locating at 33°, which can be assigned to element Se (JCPDS no. 27-602). Another peak at 44° overlaps with the peak of Co. Perhaps because most of Se in the Co–Se sample is in an amorphous phase, the peak intensity is very weak.

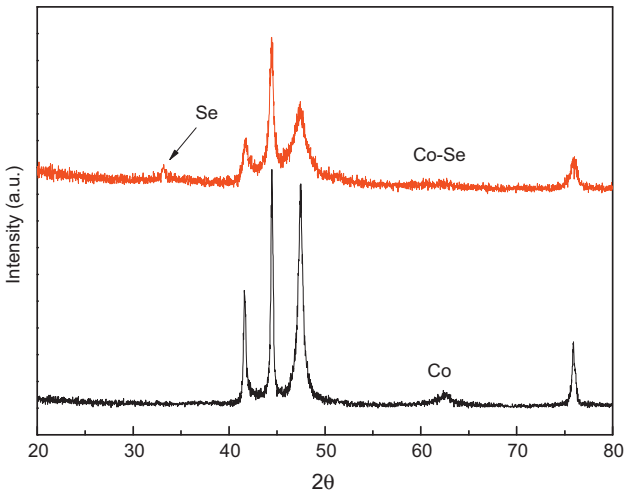

Fig. 1. XRD patterns of the prepared samples.

Fig. 2 shows the SEM images of the as-prepared Co and Co–Se samples. From Fig. 2a and b, the as-prepared Co sample shows a snowflake-like morphology, which is consistent with the result of the literature [28]. After the addition of Se, the particles become more irregular, and there is a lot of filament distributing on the surface of the particles. According to the EDS results listed below, the irregular filament is attributed to amorphous Se. These filament helps to increase the surface area of the Co–Se particles.

In order to reveal the chemical composition of the Co–Se sample, EDS spectrum is depicted in Fig. 3. As it can be seen, most of the sample is composed of Co element, while the weight ratio of Se is about 16.90%.

3.2. Effect of Se on the electrochemical performance of Co and its function mechanism

Cycle performances of the Co and Co–Se samples as negative electrodes of alkaline rechargeable batteries are displayed in Fig. 4. As it can be seen, the Co–Se electrode needs an activation process for about 40 cycles, then the discharge capacity reaches 380.8 mAh g^{-1} at a discharge current density of 50 mA g^{-1}. Even after 130 cycles, the discharge capacity can still remain at 356.5 mAh g^{-1}, with a retention rate of 93.62%. In comparison, the discharge capacity of Co sample is only about 130 mAh g^{-1} and has a tendency to decrease. Obviously, the electrochemical performance of Co–Se sample is significantly improved compared to pure Co electrode.

As it can be seen from Fig. 5, the discharge potential plateaus of the Co–Se sample gradually shift to a more negative potential with repeated cycling. At the 45th cycle, it shifts to −0.76 V and remains unaffected in the remaining cycles. In the charging process, it is observed that the first charge plateau corresponding to the reduction of Co(OH)$_2$ is lengthened and shifts to a more positive potential of around −0.94 V, while the second plateau related to hydrogen evolution is shortened and its potential almost remains unaffected [25]. Obviously, Se-incorporation leads to more active material available for electrochemical reduction reaction, as evidenced by increases in capacities corresponding to the first charge plateau.

To further investigate the electrochemical reaction mechanism, XRD patterns of the Co–Se sample after different charged/discharged states are shown in Fig. 6. As it can be seen,

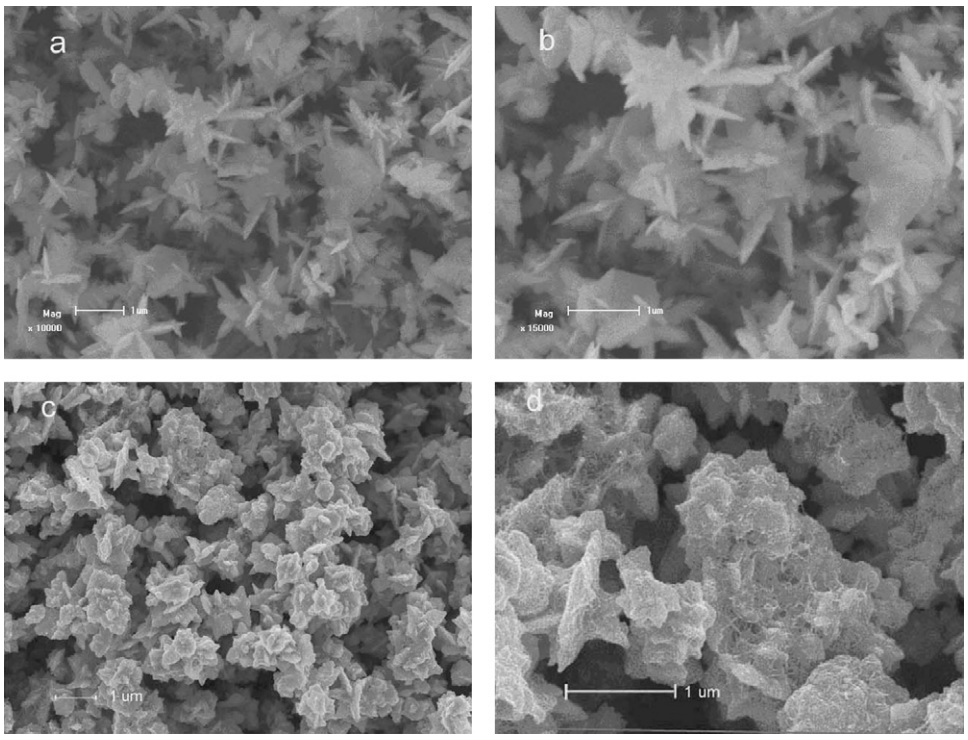

Fig. 2. SEM images of the as-prepared Co (a and b) and Co–Se (c and d) samples.

at the fully charged state of the 5th cycle, most of the diffraction peaks can be assigned to Co except a small amount of $Co(OH)_2$. After discharged, the intensity of $Co(OH)_2$ peaks strengthens while those of cobalt becomes weak, indicating that Co can be oxidated to $Co(OH)_2$ during the discharging process. Similar phase transition can be found in the 10th cycle, indicating that the discharge capacity of the electrode is mainly attributed to the electrochemical oxidation of Co. The overall reaction on the electrode can be described as $Co + 2OH^- \underset{\text{charge}}{\overset{\text{discharge}}{\rightleftharpoons}} Co(OH)_2 + 2e$.

To further confirm the electrochemical reaction process on the Co–Se sample, CV curves of the electrode at a scan rate of 2 mv s^{-1} are presented in Fig. 7. A pair of obvious redox peaks are detected, indicating that the reversible capacity is mainly based on the Faradaic redox mechanism. The curve shape and peak voltage in the tenth CV cycle are very similar to those of Co-based electrode, confirming that there occurs the same reversible reaction on them. Based on the XRD patterns after different charged/discharged states (Fig. 6), the reduction peak is due to the reduction of $Co(OH)_2$ to metallic Co while the oxidation peak should be attributed to the oxidation of metallic Co to $Co(OH)_2$.

According to the above two-electron reaction process, the theoretical electrochemical capacity of Co is 909 mAh g^{-1} by Faraday's law. As displayed in Fig. 4, the maximum reversible electrochemical capacity of the Co–Se sample is 380.8 mAh g^{-1}. After deduction of the mass contribution of Se, the calculated effective capacity of the active metallic Co is 458.2 mAh g^{-1}. So the utilization rate of Co is 50.4%, which is higher than that of pure Co (14.3%), illustrating that Se-incorporation is helpful for better utilization of Co.

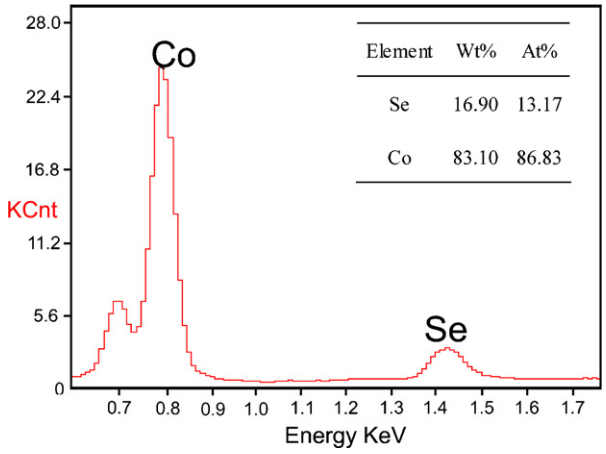

Fig. 3. EDS spectrum of the as-prepared Co–Se sample.

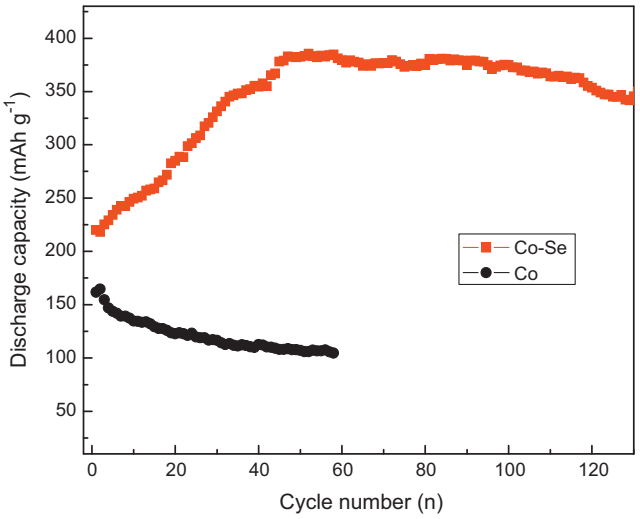

Fig. 4. Cycle performances of the samples at a discharge current density of 50 mA g^{-1}.

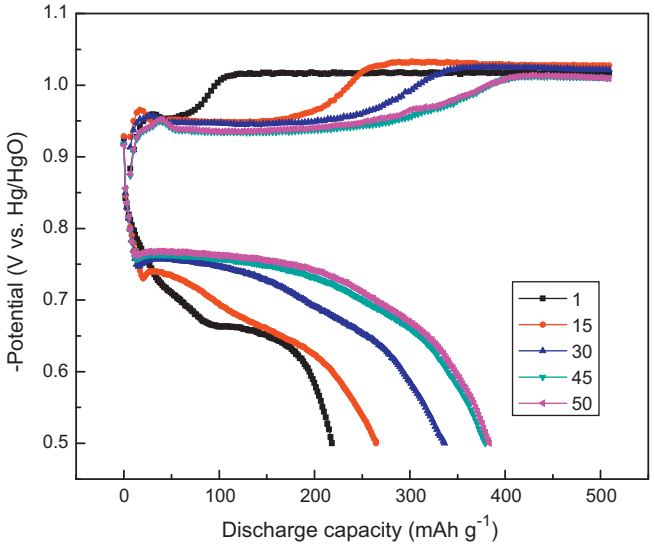

Fig. 5. Charge–discharge curves of the Co–Se sample electrode at different cycles.

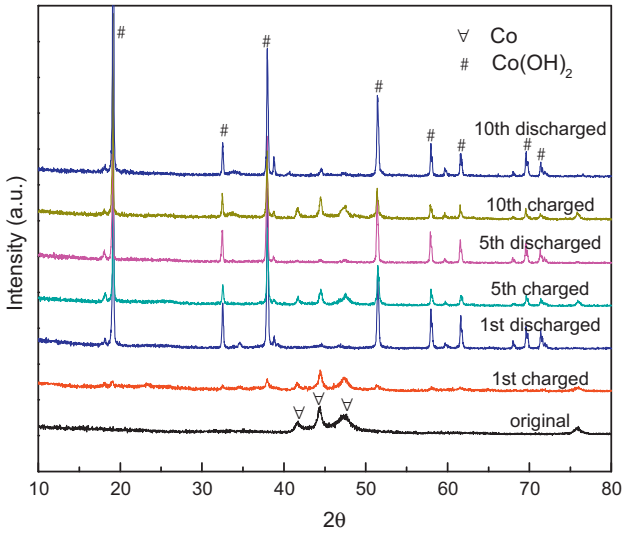

Fig. 6. XRD patterns of Co–Se sample after different charged/discharged states.

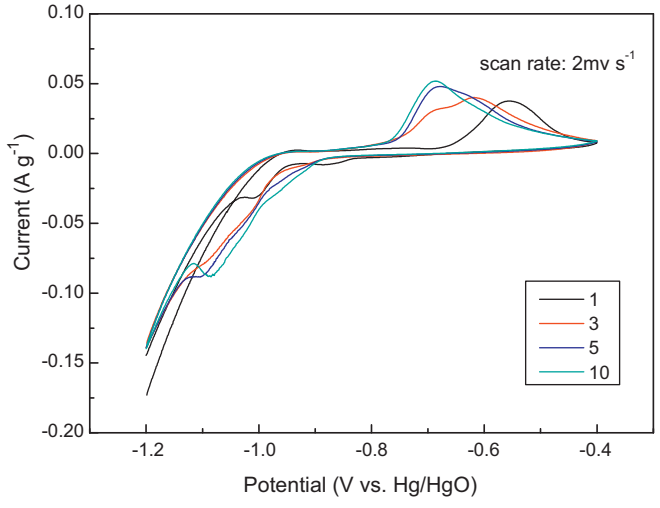

Fig. 7. CV curves of the Co–Se sample.

However, the electrochemical discharge capacity of Co is still low compared to its theoretical value. There are many factors contributing to this. First of all, as it can be seen from Fig. 6, at the fully charged states, the peaks of $Co(OH)_2$ are detected and coexist with those of Co, meaning that the partial irreversible conversion between the active metallic Co and $Co(OH)_2$ is involved in the Faradaic reaction, resulting in the low utilization of metallic Co in the Co–Se sample. Secondly, according to Haran et al. [23], there is a dissolution-precipitation balance of Co in alkaline solution:

$$Co + OH^- = CoOH_{ad} + e$$
$$CoOH_{ad} + OH^- = Co(OH)_{2,ad} + e$$
$$Co(OH)_{2,ad} + OH^- = HCoO_2^-$$

The equilibrium concentration of $HCoO_2^-$ is $>10^{-4}$ M in 6 M KOH solution at 25 °C. Establishment of this chemical equilibrium would cause a loss of active Co as well as the electrochemical discharge capacity of the Co–Se sample. Thirdly, in our work the negative electrodes are constructed through pressing the mixing powder under a pressure of 30 MPa. During this process the active material is pressed tightly together. So the contacting between active materials and the electrolyte is not so good compared to the smear method [29], leading to lower utilization of active Co.

Meanwhile, There is an activation process on the CV curves of the Co–Se sample during the initial 10 cycles. The integral area of the anodic and cathodic peaks increases gradually, in conformity with the increase of the discharge capacity in the initial several cycles. Besides, the peak voltage of the redox peaks shifts left gradually. In the first cycle, the oxidation peak in the anodic process appears at −0.56 V, in accordance with the lower discharge potential plateau in the first cycle. With cycling, the peak voltage shifts to −0.69 V in the tenth cycle. According to the ICP result, the Se content increases in the alkaline solution while decreases in the Co–Se electrode with CV cycling. So the left shift of the peak voltage originates from the electrochemical dissolution of Se in the electrode. This is similar to the result of S on the $Co(OH)_2$ electrode [24].

Fig. 8 shows the Co 2p and Se 3d XPS spectrum of the Co–Se sample after the first cycle. As it can be seen, the Co 2p peak appears at 780.2 eV before etching. After etching in Ar atmosphere for 5 min, Co 2p peak shifts to 778.3 eV, showing that Co inside the sample still exists in metallic state. In this case, the $Co(OH)_2$ just exists as a film on the surface of the sample during charge–discharge process, the film protects Co against corrosion inside the electrodes. Selenium is observed in two different forms with Se $3d_{5/2}$ binding energies of 59.7 eV and 54.6 eV. Selenium in a high oxidation state like adsorbed SeO_3^{2-} causes the first peak (59.7 eV). The second peak (54.6 eV) is reported for elemental selenium [30,31]. However, the intensity of Se $3d_{5/2}$ peak at 54.6 eV varies before and after etching process. Before etching, the peak at 54.6 eV is weak, indicating that part of Se is oxidized to SeO_3^{2-}, because of the poor electronegativity of Se (−0.366 V vs. NHE), the oxidation proceeds slowly, after the first discharging, much of Se still remains at 0 oxidation state. However, after etching in Ar atmosphere, the peak at 54.6 eV becomes stronger, indicating that Se element still mainly exists in 0 oxidation inside the sample.

From the analysis above, we can take such an assumption for the mechanism of Se on the process as follows: firstly, the introduction of Se enhances the surface area of the Co–Se particles. Secondly, as the amorphous Se dissolving into the KOH solution, new interspaces between the active electrode material and the electrolyte are produced. More interspaces are correlate to larger contact area with the alkaline solution, which significantly enhances the electrochemical reaction efficiency. However, owing to the slow dissolution rate of Se into the electrolyte, it takes 40 cycles to activate the Co–Se sample electrode.

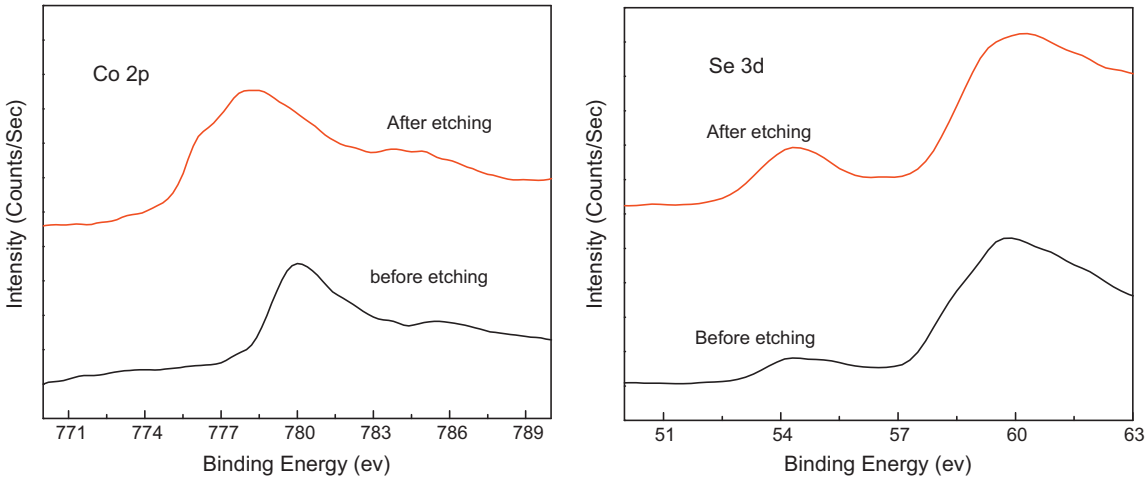

Fig. 8. XPS spectrum of Co and Se of Co–Se sample electrode after the first cycle.

4. Conclusions

This paper describes the potentiality of Se incorporation in enhancing the electrochemical performance of Co electrode. The function mechanism of Se is similar to the result of previously reported B and S. It is proved that Co–Se sample has potential to be a negative electrode material of alkaline rechargeable batteries. Se-incorporation can be obtained through other methods, for example directly mixing of commercial Co powders and Se powders and similar results are obtained. This methodology can also be used to choose other inactive materials beneficial for enhancing the electrochemical performance of Co-based alkaline rechargeable batteries.

Acknowledgements

This work was financially supported by 973 program (2010CB631303), NSFC (50971071, 51071087) and MOE Innovation Team (IRT0927).

References

[1] A.K. Shukla, S. Venugopalan, B. Hariprakash, J. Power Sources 100 (2001) 125–148.
[2] E.J. Casey, A.R. Dubois, P.E. Lake, W.J. Moroz, J. Electrochem. Soc. 112 (1965) 371–383.
[3] D.C.R. Espinosa, J.A.S. Tenório, J. Power Sources 136 (2004) 186–190.
[4] K. Micka, Z. Zabransk, J. Power Sources 19 (1987) 315–323.
[5] K. Vijayamohanan, T.S. Balasubramanian, A.K. Shukla, J. Power Sources 34 (1991) 269–285.
[6] N. Comisso, G. Mengoli, J. Appl. Electrochem. 37 (2007) 949–959.
[7] W.Z. Shen, S.M. Han, Y.L.J.Z. Song, Q. Tong, Electrochim. Acta 56 (2010) 959–963.
[8] H. Huang, L. Zhang, W.K. Zhang, Y.P. Gan, H. Shao, J. Power Sources 184 (2008) 663–667.
[9] H. Miao, W.G. Wang, J. Alloys Compd. 508 (2010) 592–598.
[10] Y.H. Zhang, F. Hu, Z.G. Li, K. Lu, S.H. Guo, X.L. Wang, J. Alloys Compd. 509 (2011) 294–300.
[11] Y.F. Liu, H.G. Pan, M.X. Gao, Q.D. Wang, J. Mater. Chem. 21 (2011) 4743–4755.
[12] Y.D. Wang, X.P. Ai, H.X. Yang, Chem. Mater. 6 (2004) 5194–5197.
[13] D.W. Song, Y.J. Wang, Y.P. Wang, L.F. Jiao, H.T. Yuan, Electrochem. Commun. 10 (2008) 1486–1489.
[14] Y. Liu, Y.J. Wang, L.L. Xiao, D.W. Song, L.F. Jiao, H.T. Yuan, Electrochem. Commun. 9 (2007) 925–929.
[15] G. He, L.F. Jiao, H.T. Yuan, Y.Y. Zhang, Y.J. Wang, Electrochem. Commun. 8 (2006) 1633–1638.
[16] Y.L. Cao, W.C. Zhou, X.Y. Li, X.P. Ai, X.P. Gao, H.X. Yang, Electrochim. Acta 51 (2006) 4285–4290.
[17] Y. Wang, J.M. Lee, X. Wang, Int. J. Hydrogen Energy 35 (2010) 1669–1673.
[18] Z.W. Lu, S.M. Yao, G.R. Li, T.Y. Yan, X.P. Gao, Electrochim. Acta 53 (2008) 2369–2375.
[19] S.M. Yao, K. Xi, G.R. Li, X.P. Gao, J. Power Sources 184 (2008) 657–662.
[20] X.P. Gao, S.M. Yao, T.Y. Yan, Z. Zhou, Energy Environ. Sci. 2 (2009) 502–505.
[21] Q.H. Wang, L.F. Jiao, H.M. Du, W.X. Peng, D.W. Song, Y.J. Wang, H.T. Yuan, Electrochim. Acta 56 (2011) 1106–1110.
[22] H.M. Du, L.F. Jiao, Q.H. Wang, W.X. Peng, D.W. Song, Y.J. Wang, H.T. Yuan, J. Power Sources 196 (2011) 5751–5755.
[23] B.S. Haran, B.N. Popov, R.E. White, J. Electrochem. Soc. 145 (1998) 3000–3007.
[24] D.W. Song, Y.J. Wang, Q.H. Wang, Y.P. Wang, L.F. Jiao, H.T. Yuan, J. Power Sources 195 (2010) 7115–7119.
[25] Y. Liu, Y.J. Wang, L.L. Xiao, D.W. Song, Y.P. Wang, L.F. Jiao, H.T. Yuan, Electrochim. Acta 53 (2008) 2265–2271.
[26] D.S. Lu, W.S. Li, C.L. Tan, R.H. Zeng, Electrochim. Acta 55 (2009) 171–177.
[27] J.A. Johnson, M.L. Saboungi, P. Thiyagarajan, R. Csencsits, D. Meisel, J. Phys. Chem. B 103 (1999) 59–63.
[28] Z.T. Liu, X. Li, Z.W. Liu, J. Lu, Powder Technol. 189 (2009) 514–519.
[29] Q.H. Wang, L.F. Jiao, H.M. Du, Q.N. Huan, W.X. Peng, D.W. Song, Y.J. Wang, H.T. Yuan, J. Mater. Chem. (2011), doi:10.1039/c1jm11626f.
[30] http://www.lasurface.com.
[31] H. Schulenburg, M. Hilgendorff, I. Dorbandt, J. Radnik, P. Bogdanoff, S. Fiechter, M. Bron, H. Tributsch, J. Power Sources 155 (2006) 47–51.